

THE HUBBLE-TYPE OUTFLOWS FROM THE HIGH-EXCITATION, POLYPOLAR PLANETARY NEBULA NGC 6302

J. MEABURN, J. A. LÓPEZ, AND W. STEFFEN

Instituto de Astronomía, Universidad Nacional Autónoma de México, Campus Ensenada, Apartado Postal 877, 22800 Ensenada, Mexico

AND

M. F. GRAHAM AND A. J. HOLLOWAY

Jodrell Bank Observatory, University of Manchester, Macclesfield SK11 9DL, UK

Received 2005 July 8; accepted 2005 July 26

ABSTRACT

Spatially resolved profiles of the $H\alpha$ and $[N\text{ II}]$ lines have been obtained at unprecedented signal-to-noise ratios over the outflowing lobes of the high-excitation, polypolar planetary nebula NGC 6302. A deep image in the light of $[N\text{ II}] \lambda 6584$ was also obtained of the extremities of the prominent northwestern lobe. The Manchester Echelle Spectrometer combined with the 2.1 m San Pedro Martir telescope (Mexico) was used for these observations. First, an accurate value of the systemic heliocentric radial velocity of $V_{\text{sys}} = -29.8 \pm 1 \text{ km s}^{-1}$ has been established. Also, from “velocity ellipses” across its diameter from previous observations, the parallel-sided northwestern lobe is shown to have a circular section with a tilt of its axis to the plane of the sky of $12^\circ 8'$. With this starting point the position-velocity arrays of profiles have been very closely simulated, using the SHAPE code, with Hubble-type outflows. The faint extremities of the northwestern outflow are shown to be expanding at $\geq 600 \text{ km s}^{-1}$. The prominent lobes of NGC 6302 have then been generated in an eruptive event with a dynamical age of 1900 yr for an expansion proper-motion distance of $1.04 \pm 0.16 \text{ kpc}$, as measured here by comparing a 1956 image with one taken in 2002. Kinematical evidence of a high-speed “skirt” around the nebular core, expanding nearly orthogonally to the lobes, is also presented, as are the unusual motions at the western extremities of the northwestern lobe.

Key word: planetary nebulae: individual (NGC 6302)

1. INTRODUCTION

NGC 6302 (PN G349.5+01.0) is a polypolar planetary nebula (PN) that was described and drawn as early as 1907 by Barnard (1907). The many estimations of the distance to NGC 6302 range from 0.15 to 2.4 kpc, although Gómez et al. (1989), from a radio expansion proper-motion measurement of the bright nebular core, give a firm lower limit to the distance of $0.8 \pm 0.3 \text{ kpc}$ (see § 3.3) and give a distance of $2.2 \pm 1.1 \text{ kpc}$ from measurements of the pressure-broadening of radio recombination lines.

The complex morphology of NGC 6302 is clearly evident in the photography of Evans (1959) and Minkowski & Johnson (1967); it is approximately bipolar, consisting of two principle lobes. A dark lane covers the waist of the nebula and has prevented the optical detection of the central stellar system. This dark lane has been observed in $H\text{ I}$ absorption and is bright in a wide range of emissions, e.g., polycyclic aromatic hydrocarbon, free-free radio, blackbody infrared and microwave, $H\text{ I}$, and H_2 . (Rodríguez et al. 1985; Matsuura et al. 2005). A massive ($0.5\text{--}3 M_\odot$) toroid of material must surround and obscure ($A_V = 5\text{--}7 \text{ mag}$) the central star, with the line and free-free emission coming from close to the star and the neutral dusty material causing $H\text{ I}$ and optical absorption farther out. Rodríguez et al. (1985) also argue for the existence of an extended neutral hydrogen halo surrounding NGC 6302.

Feibelman (2001) suggests that the ultraviolet *IUE* continuum spectrum, uncorrected for interstellar extinction, indicates that the central $O\text{ VI}$ -type white dwarf has a G-type companion. However, although Barral et al. (1982) detect the same continuum in their own *IUE* spectrum, they conclude, after correction for logarithmic interstellar extinction coefficients of c between 1.0 and 1.59, that it is scattered radiation from the hot star. However, a symbiotic status remains possible when compared with

the similar, although lower excitation, nebula Menzel 3 (Mz 3; Bains et al. 2004; Schmeja & Kimeswenger 2001).

A large range of ionization energies is present in the extended lobes of the nebula. Optical and infrared line emission have been observed from neutral species such as $[O\text{ I}]$, through ionized species such as $H\alpha$, $[N\text{ II}]$, up to $[O\text{ III}]$, He II , $[Ne\text{ V}]$, and even as high as $[Si\text{ VII}]$ (Meaburn & Walsh 1980b; Pottasch et al. 1985; Ashley & Hyland 1988; Feibelman 2001); in fact, NGC 6302 is one of the highest excitation class of PNe known. As a result, if the nebula is being photoionized by the obscured central star, the star must be extremely hot ($\geq 10^5 \text{ K}$; e.g., Pottasch et al. 1985; Ashley & Hyland 1988; Casassus et al. 2000). A stellar wind (Meaburn & Walsh 1980a) could instead be shock-exciting the surrounding gas, but Barral et al. (1982) have concluded that radiative ionization is almost certainly predominant due to NGC 6302's close spectral similarity to other radiatively ionized, high-excitation PNe. The 800 km s^{-1} broad wings (Meaburn & Walsh 1980a) to the $[Ne\text{ V}] \lambda 3426$ line profiles were originally considered to be direct manifestations of this particle wind; Barral et al. (1982) demonstrate that this is improbable and that their origin in electron scattering or even as instrumental artifacts should be considered. Feibelman (2001), however, identifies some very high excitation, coronal-type spectral features that cannot be produced by radiative ionization by the central star and proposes that shocks must play a part in their generation. The detection of centrosymmetric polarization of the nebular radiation (King et al. 1985) suggests that the bright core light is being scattered by the dust content of the outflowing lobes.

The density-sensitive $[Ar\text{ IV}] \lambda\lambda 4711, 4740$ intensity ratio gives an electron density $n_e \approx 80,000 \text{ cm}^{-3}$ immediately adjacent to the dark waist, and other density-sensitive ratios, which work in less dense regimes, show that n_e falls to $\approx 1000 \text{ cm}^{-3}$ in the extended lobes of NGC 6302 (Barral et al. 1982). Meaburn

& Walsh (1980b), however, identify a knot in the extremities of the western lobe (knot 1 in Fig. 2*b*) that has $n_e \approx 3000 \text{ cm}^{-3}$.

The electron temperature of the nebula adjacent to the dark waist itself has been estimated a number of times using diagnostic spectral line intensity ratios. Oliver & Aller (1969) found temperatures in the range 15,200–22,000 K at various points over the two principle inner lobes. Danziger et al. (1973) found a temperature of 17,400 K from the infrared continuum emission. Aller et al. (1981) observed this brightest portion of the nebula and adopted 16,400 K after they found that a number of nebular line diagnostics converge on this value. These high temperatures (10,000 K is usually anticipated for ionized circumstellar gas) are consistent with $20,400 \pm 4000 \text{ K}$, derived from the relative widths of the $\text{H}\alpha$ and $[\text{N II}] \lambda 6584$ emission-line profiles (Barral et al. 1982).

Evans (1959) initially suggested that the form of NGC 6302 suggests dynamic interaction with the ambient medium, and the kinematics were first investigated by Minkowski & Johnson (1967), who found clear line-splitting in the lobes: it was immediately obvious that NGC 6302 is not undergoing spherically symmetric expansion. Minkowski & Johnson (1967) and Elliott & Meaburn (1977) showed that the expansion in the inner lobes, in particular their neutral $[\text{O I}] \lambda 6300$ -emitting component, is superposed on a velocity gradient across NGC 6302. The kinematics of the nebula were first thoroughly investigated by Meaburn & Walsh (1980b) using long-slit spectroscopy. The distribution of radial velocities was found to be consistent with the existence of a number of cavities flowing out from the center of the nebular waist, hence the polypolar description of the nebula. The dominant “closed” cavity is to the northwest, although nebular emission certainly extends in this direction much farther than suggested in the previous imagery. Early indications were found by Meaburn & Walsh (1980b) that the kinematics and morphology of this extreme region are not easily explicable within a closed-lobe model with simple outflowing walls; consequently, new, very deep, spatially resolved position-velocity (PV) arrays of profiles of the $[\text{N II}] \lambda 6584$ nebular emission line over NGC 6302 have been obtained. These new observations have taken advantage of the technical improvements in the 25 years since those of Meaburn & Walsh (1980b), not least a CCD replacing the earlier photon counting detector and the use of an echelle grating in the spectrometer, along with up-to-date displays of the data.

In these most recent observations, particular, although not exclusive, attention has been paid to the far tip of the northwestern lobe. A deep $[\text{N II}] \lambda 6584$ image has been obtained to highlight the farthest extension of this part of the nebula. Morphological and kinematical modeling have also been performed to elucidate more clearly the structure and motions of these nebular lobes. A firm expansion proper-motion distance has been established by comparing a 1956 image from Evans (1959) with the most recent one, obtained in the present work.

2. OBSERVATIONS AND RESULTS

The present observations were made with the Manchester Echelle Spectrometer (MES; see Meaburn et al. 1984, 2003) combined with the 2.1 m San Pedro Martir (SPM) telescope on 2001 May 17/18 and 2002 May 10/12. A SITE CCD was the detector with $1024 \times 1024 \text{ } 24 \mu\text{m}$ pixels, although 2×2 binning was employed throughout the observations.

2.1. Imagery

MES-SPM has a limited imaging capability with a retractable plane mirror isolating the echelle grating and a clear area (here $4'.37 \times 5'.32$) replacing the spectrometer slit. The image

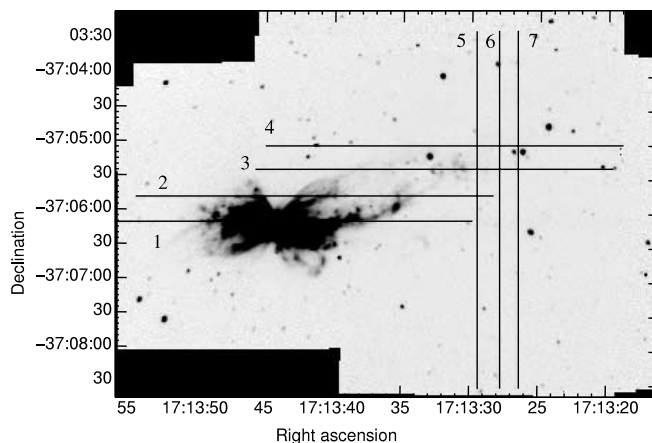


FIG. 1.—Slit positions 1–7 against a negative image of NGC 6302 in the light of $\text{H}\alpha + [\text{N II}]$ (J2000.0).

in Figure 1 is a mosaic of those snapshot images through the 90 \AA bandwidth $\text{H}\alpha + [\text{N II}]$ interference filter taken immediately before obtaining spatially resolved long-slit spectra of these lines (see § 2.2). The image in Figure 2 is a subset from this larger

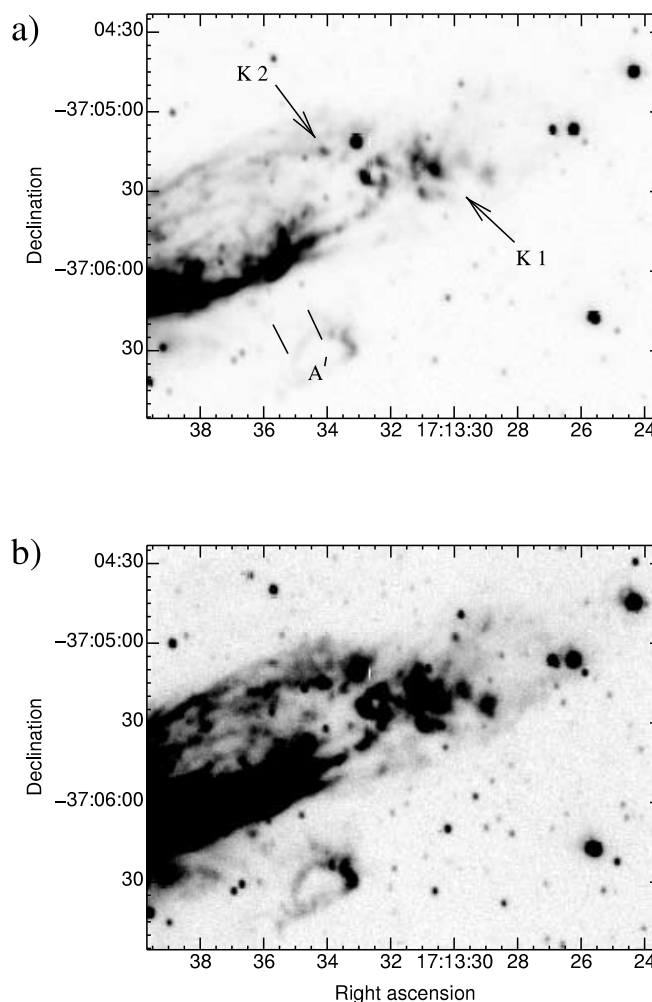


FIG. 2.—Western lobe of NGC 6302 (2002 May 12) through a narrow filter centered on $[\text{N II}] \lambda 6584$. (a) Light presentation revealing the brighter features. The high-density knot 1 from Meaburn & Walsh (1980b) is marked K1, and the band A', which gives the velocity ellipse in Fig. 13*b*, is indicated. The outward proper motion of knot 2 (marked K2) has been measured. (b) Deep presentation of the same image to reveal the faintest structure.

TABLE 1

SLIT WIDTHS, ORIENTATIONS, AND EXPOSURE TIMES USED TO OBTAIN LONG-SLIT SPECTRA OF NGC 6302

Slit Position	Slit Orientation	Slit Width (μm)	Exposure Time (s)
1.....	EW	150	300
2.....	EW	150	1200
3.....	EW	150	1800
4.....	EW	150	1800 + 2400
5.....	NS	300	2 \times 1800
6.....	NS	300	2 \times 1800
7.....	NS	300	2 \times 1800

NOTE.—For the positions shown in Fig. 1.

field obtained on 2002 May 12 with this MES-SPM imaging configuration but covering only the western lobe of NGC 6302. The integration time was 900 s. The coordinates (J2000.0) were added using the Starlink GAIA software. The 10 Å bandwidth interference filter that was employed transmits only the [N II] λ 6584 emission line.

2.2. Long-Slit Spectroscopy

Spatially resolved, long-slit line profiles were obtained with MES-SPM along the lines marked 1–7 in Figure 1. The details of all spectroscopic observations are listed in Table 1. In this spectroscopic mode MES-SPM has no cross-dispersion; consequently, for the present observations a filter of 90 Å bandwidth was used to isolate the 87th echelle order containing the H α and [N II] λ 6548, 6584 nebular emission lines.

The 512 increments, each 0".624 long, give a total projected slit length of 5'.32 on the sky. Seeing was always $\approx 1''$ during these observations. A 150 μm wide ($\equiv 11 \text{ km s}^{-1}$ and 1".9) slit was employed for the brighter nebulosity nearer the nebular core. For the spectrometry of the faintest but high-speed gas this slit was changed to one that is 300 μm wide ($\equiv 22 \text{ km s}^{-1}$ and 3".8) to achieve sufficient signal-to-noise ratio, although at the expense of spectral resolution.

The spectral data were bias-corrected, cleaned, etc., in the usual way using the Starlink FIGARO and KAPPA software packages. All spectra were calibrated in heliocentric radial velocity (V_{hel}) to $\pm 1 \text{ km s}^{-1}$ accuracy against the spectrum of a thorium/argon lamp.

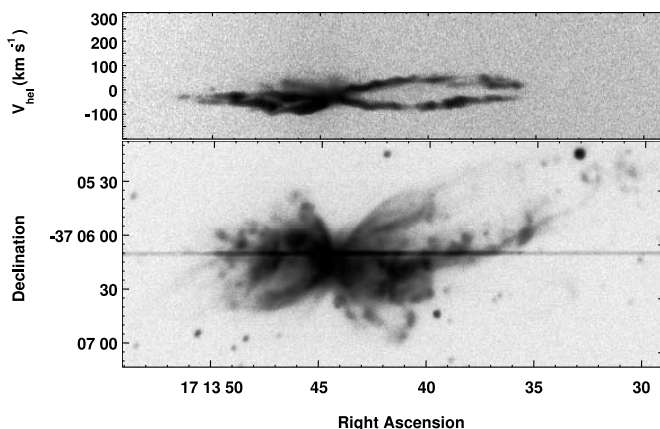


FIG. 3.—Top: PV array of [N II] λ 6584 profiles for the east-west slit position 1. This should be compared in detail with the image of the slit across the H α + [N II] image of NGC 6302 in the bottom panel.

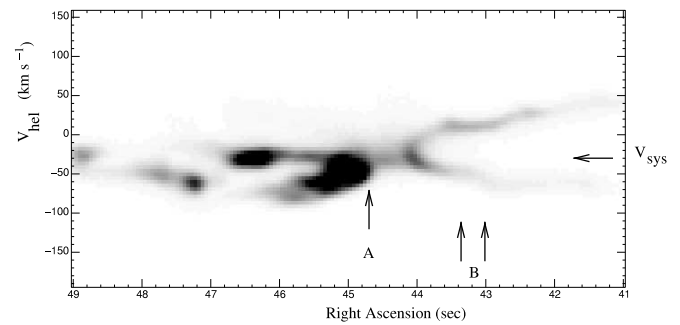


FIG. 4.—Light presentation of a subset of the PV array of [N II] λ 6584 profiles for slit position 1 in Fig. 3 that crosses the nebular core, where V_{sys} is shown by the horizontal arrow. The positions where the line profiles in Fig. 11 were obtained are marked A and B.

The negative gray-scale representations of those parts of the PV arrays for slit positions 1–7 are shown in Figures 3–10. Only the [N II] λ 6584 profiles are shown. These are compared in each case with the snapshot image of the sky and slit taken immediately before the spectroscopic integration through the same 90 Å bandwidth filter. The origins of spectral features are precisely identified by this technique. Sample H α and [N II] λ 6584 line profiles for positions A and B in Figure 4 are shown in Figure 11; similarly, [N II] λ 6584 profiles from positions C–H in Figures 5–9 are shown in Figure 12.

3. NEW KINEMATICAL AND MORPHOLOGICAL FEATURES

3.1. Systemic Velocity

All kinematical features must be discussed with respect to the systemic heliocentric radial velocity V_{sys} . The radial velocities of the two [N II] λ 6584 line profiles on either side of the central dark lane and closest to its edges for slit position 1 (Fig. 4) afford the opportunity to measure V_{sys} with some certainty; they are both single, narrow, and reasonably Gaussian in shape. Gaussian fitting shows that the western profile is centered on $V_{\text{hel}} = -34.0 \text{ km s}^{-1}$ and the eastern profile shown in Figure 11a is centered on -25.5 km s^{-1} , with both widths (including instrumental broadening) $\approx 31 \text{ km s}^{-1}$. If we assume that these central velocities are evenly distributed around V_{sys} , then a value of $V_{\text{sys}} = -29.8 \pm 1 \text{ km s}^{-1}$ is therefore indicated for the whole nebular complex. The rest wavelength of the [N II] λ 6584 line is taken as $6583.45 \pm 0.01 \text{ \AA}$ (calibrated against H α at 6562.82 Å) in these

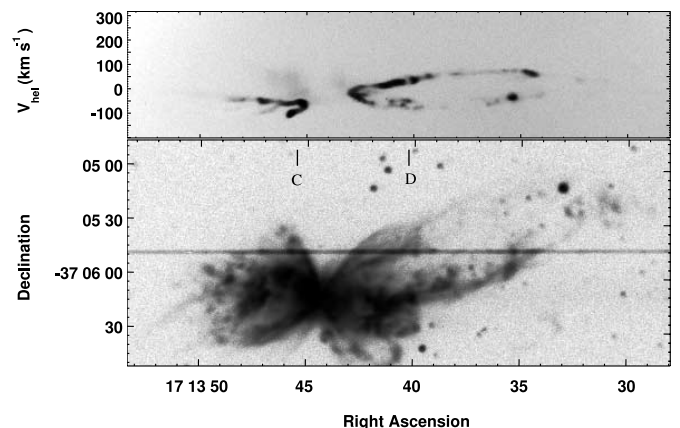


FIG. 5.—Same as Fig. 3 but for slit position 2. The profiles from C and D are shown in Fig. 12.

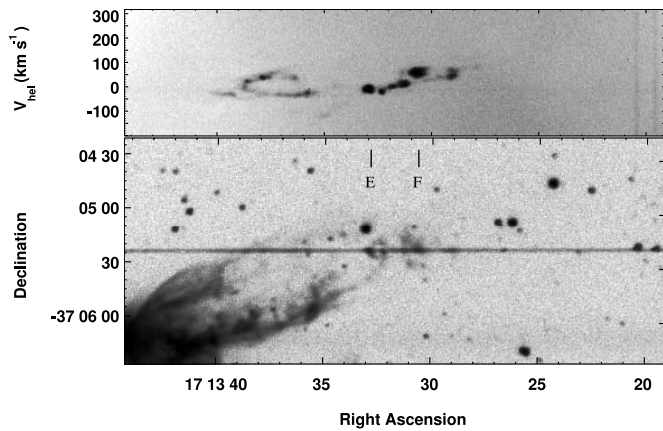


FIG. 6.—Same as Fig. 3 but for slit position 3. The profiles from E and F are shown in Fig. 12.

calculations (Meaburn et al. 1996), and the less accurate $[\text{N II}] \lambda 6584$ rest wavelength used by Meaburn & Walsh (1980b) accounts for the approximately -9 km s^{-1} difference between the value of V_{sys} given in that paper and the value reported here.

3.2. The Prominent Northwestern Lobe

A starting point for the understanding of the morphology and kinematics of all the lobes of NGC 6302, including their extremities, is the derivation of the detailed form and behavior of the most prominent northwestern lobe. In Figure 2 it can be seen that for a large part of its length the walls of the northwestern lobe are parallel. This is approximately depicted in Figure 13a. The PV arrays in Figures 3, 5, and 6 clearly show both the radial expansion of this lobe and the tilt to more positive radial velocities away from the central star as found by Meaburn & Walsh (1980b). “Velocity ellipses” indicative of radial expansion with a nearly circular section were shown clearly by Meaburn & Walsh (1980b), as depicted schematically in Figure 13b for the A' cut across the northwestern lobe also marked in Figure 2a. Aspects of this northwestern lobe of NGC 6302, i.e., its parallelism and velocity ellipses across its width, are found in the lobes of the comparable object Mz 3 (López & Meaburn 1983; Meaburn & Walsh 1985).

The angle $\phi = 12.8^\circ$ can be directly measured from Figure 2b and is sketched in the (X, Y) -plane in Figure 13a. The separation of the lobe edges along the A' cut was measured on the image with GAIA, and simple geometry gives 2ϕ . As a circular section is indicated by the velocity ellipses and this angle is small, then to a reasonable approximation the structure and kinematics of the lobe in the (X, Z) -plane is shown in Figure 13c (the observer is below Fig. 13c). The measured radial velocity differences with respect to V_{sys} from Figure 4 of Meaburn & Walsh (1980b) are $\delta V_1 = 0 \text{ km s}^{-1}$, $\delta V_2 = 59 \text{ km s}^{-1}$, and $\delta V_3 = 117 \text{ km s}^{-1}$, which first implies that the nearside of the lobe along the A' cut is flowing in the plane of the sky with expansion velocity V and then that the lobe axis is $\phi = 12.8^\circ$ to the plane of the sky, as shown in Figure 13c.

As $V = \delta V_3 [\sin(2\phi)]^{-1}$ and $\delta V_2 (\sin \phi)^{-1}$, a value of $V = 263 \pm 5 \text{ km s}^{-1}$ is given at position A' (1.71 from the central star) and along the directions shown in Figure 13c. The $[\text{N II}]$ image in Figure 2 and the spectacular one by Corradi, obtained with the 3.6 m La Silla telescope,¹ are also significant to the dynamical interpretation because they suggest that the walls of the northwestern lobe are not uniformly filled with outflowing

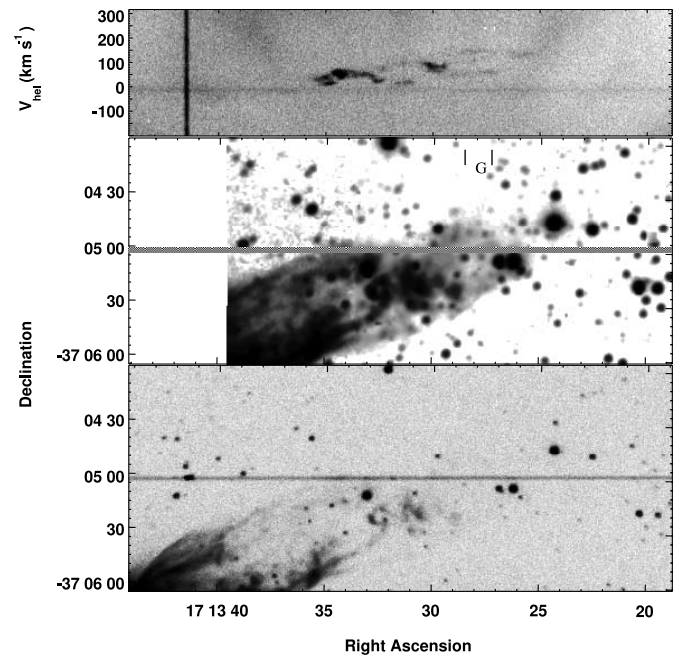


FIG. 7.—Same as Fig. 3 but for slit position 4. The profile from the band G is shown in Fig. 12. The central panel is a deep image taken at the time of the spectral observation.

gas: long filaments within these walls project back to the central star. Also, there are gaps in the PV arrays, most notably where the slit crosses the western edge of this lobe in Figure 3.

3.3. Expansion Distance

After distance (D in kiloparsecs) determinations of PNe based on parallax, the most certain method is by measurements of expansion proper motions ($\delta\theta$ in mas yr^{-1}), particularly when the expansion tangential velocities (V_t in km s^{-1}) are both high and well known. For the outflow depicted in Figure 13, $V_t = V \cos \phi$, so

$$D \delta\theta = 216.8 V \cos \phi. \quad (1)$$

Gómez et al. (1989, § 1) attempted this measurement of D for the core of NGC 6302, where the expansion velocity is only 10 km s^{-1} . In the present work (Fig. 13, § 4) the northwestern lobe velocity is found to be both high ($V = 263 \text{ km s}^{-1}$ at A' in Fig. 2a) and directed along low angles to the plane of the sky. The expansion proper motion of $\delta\theta = 56D^{-1} \text{ mas yr}^{-1}$ is then predicted by the parameters in § 3.2 for position A' at 1.71 from the nebular center in Figure 2a.

Even a simple visual comparison of the $\text{H}\alpha + [\text{N II}]$ image taken by Evans (1959) on 1956 August 8 of NGC 6302 with the $[\text{N II}] \lambda 6584$ image in Figure 2a reveals significant angular shifts outward with time of many of the nebular features at the extremities of the northwestern lobe. As the $[\text{N II}] \lambda\lambda 6548, 6584$ lines combined are 2–3 times as bright as $\text{H}\alpha$ in these lobes, these images are then reasonably comparable. The most certain measurement of this shift is for the knot marked K2 in Figure 2a, since it is bright, compact, and conveniently between two close stellar images.

The position of K2 relative to these stars was made by ruler off an enlargement of Evan’s (1956) published image to an accuracy of $0.5''$. Its position relative to the same two stars was measured to far higher accuracy using GAIA on the data array for the 2002 image in Figure 2a. A shift outward is detected along a line to the nebular center of $3.26 \pm 0.5''$ in the 45.762 yr between the two

¹ See <http://sci.esa.int/science-e/www/object/index.cfm?fobjectid=34985>.

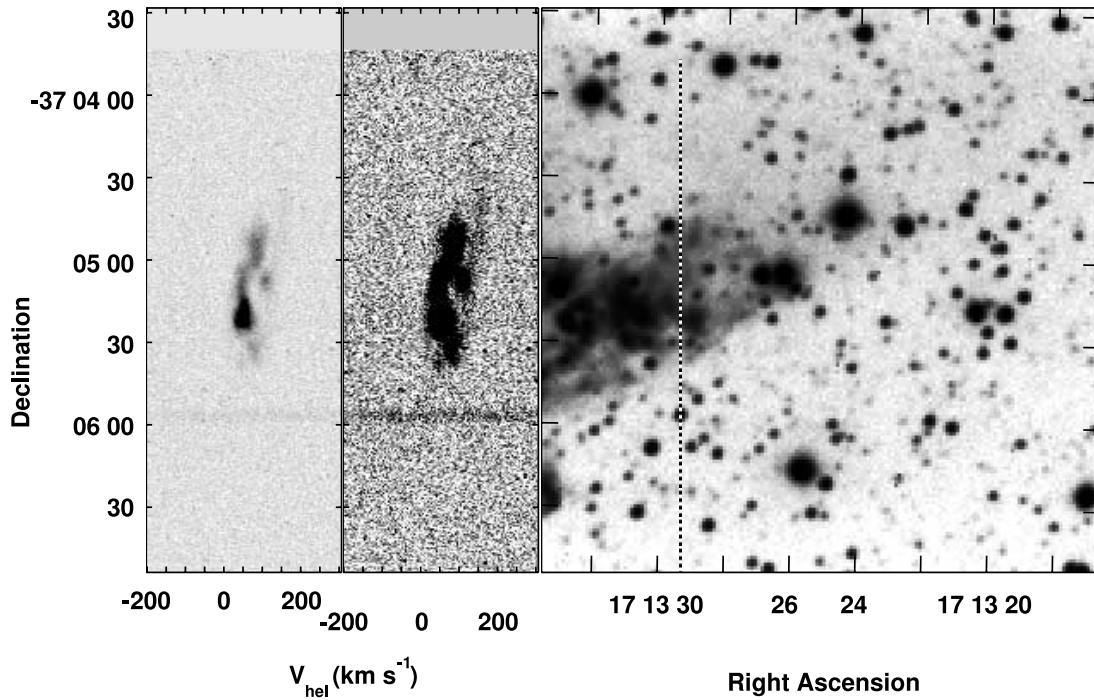


FIG. 8.—Light and deep presentations of the [N II] $\lambda 6584$ PV array of profiles along the north-south slit position 5 (*two leftmost panels*). These should be compared to the slit position shown as a dashed line against the H α + [N II] image of NGC 6302 in the right panel.

images to give $\delta\theta = 70.4 \pm 10 \text{ mas yr}^{-1}$. As the angular distance from the core of K2 is $2'24$, compared with $1'71$ for position A', and assuming a Hubble-type expansion of the lobe (see § 4), then the predicted value of $\delta\theta = 73D^{-1} \text{ mas yr}^{-1}$, since now $V = 345 \text{ km s}^{-1}$ to give $D = 1.04 \pm 0.16 \text{ kpc}$ as the distance to NGC 6302. Somewhat lower accuracy measurements of knots and filaments in the vicinity of K2 indicate very similar proper-motion displacements, confirming that those of K2 are not anomalous. Obviously, if the original 1956 plate can be scanned and the results compared in detail with the data array for

Figure 2a, both a more accurate distance can be established and the Hubble-type nature of the outflow can be tested independently of the kinematical modeling in § 4.

3.4. The Lobe Extremities

The complexities of the extremities of the northwestern lobe are revealed in the PV arrays of the [N II] $\lambda 6584$ profiles in Figures 7–10, as well as in the deep image in Figure 2b. Separate expansions across this region are particularly apparent in

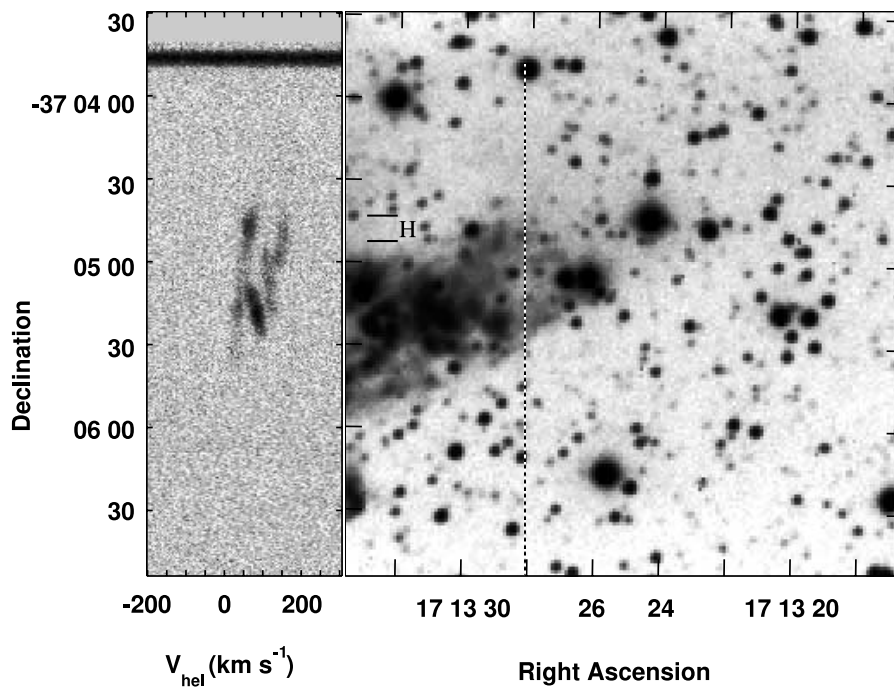


FIG. 9.—Same as Fig. 8 but for slit position 6. Only one presentation of the PV array is shown. The profile from the band H is shown in Fig. 12.

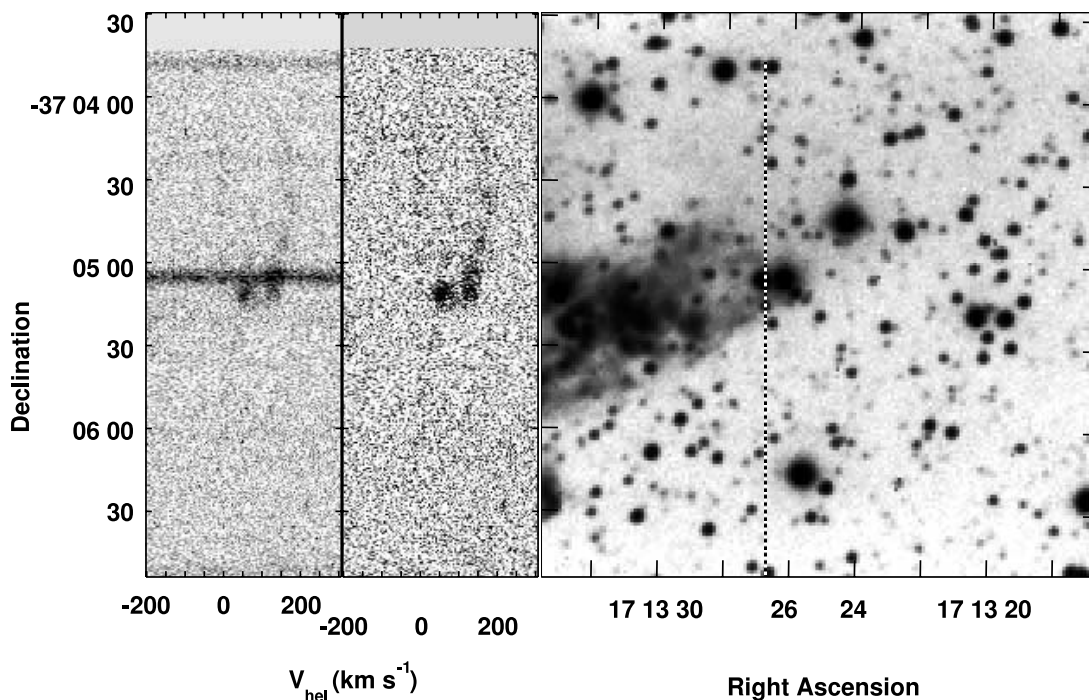


Fig. 10.—Same as Fig. 8 but for slit position 7. The confusing stellar spectrum (*horizontal band*) is removed from the right panel of the PV array in this display.

Figure 7, with values of V_{hel} reaching $\approx 175 \text{ km s}^{-1}$ in Figures 8–10, which is $\approx 205 \text{ km s}^{-1}$ with respect to V_{sys} (and see the [N II] $\lambda 6584$ profiles in Fig. 12 for positions G and H). This behavior is obviously more complex than that depicted for the principal northwestern lobe in Figure 13. Radial expansion of a single coherent feature no longer seems present, because separate “sheets” of material with different radial velocities can be seen in the PV arrays. This extremity is westward of the group of knots of which knot 1 (indicated in Fig. 2a) is a member. The more eastern knot has a radial velocity close to V_{sys} (Fig. 6 and [N II] $\lambda 6584$ profiles for position E in Fig. 12), and it appears to be the region in which the prominent northwestern lobe changes its character.

Knot 1 (position F in Figs. 6 and 12), however, has a significantly more positive velocity.

3.5. High-Speed Skirt

High-speed velocity components in the [N II] $\lambda 6584$ profiles are revealed in Figure 5 and in the profile marked C in Figure 12. Positive velocity wings are also present in the profiles in Figure 11a from position A in Figure 4. These continuous

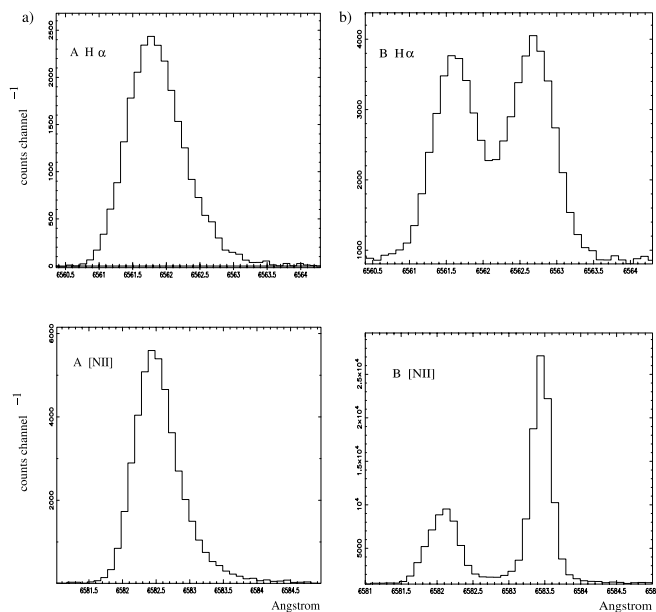


FIG. 11.—H α and [N II] $\lambda 6584$ line profiles from positions (a) A and (b) B in Fig. 4.

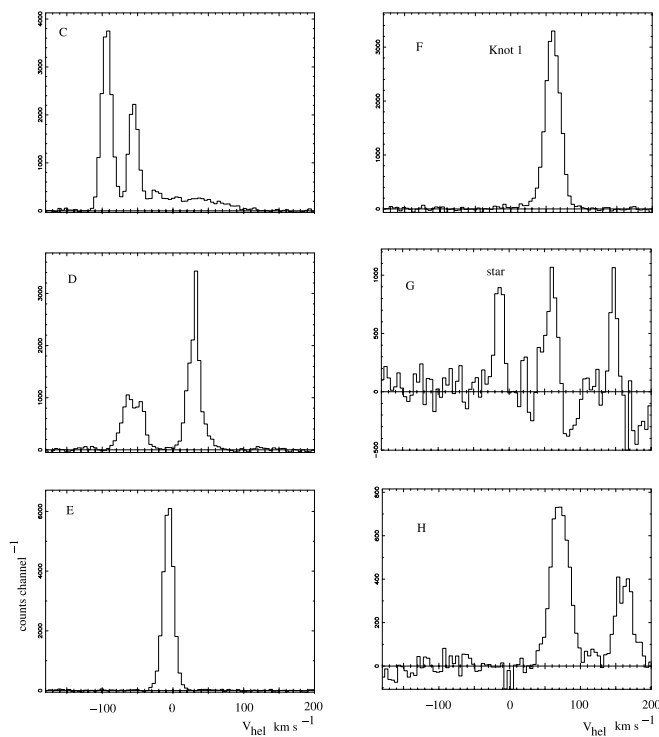


FIG. 12.—Sample [N II] $\lambda 6584$ line profiles from positions C–H in Figs. 5, 6, 7, and 9.

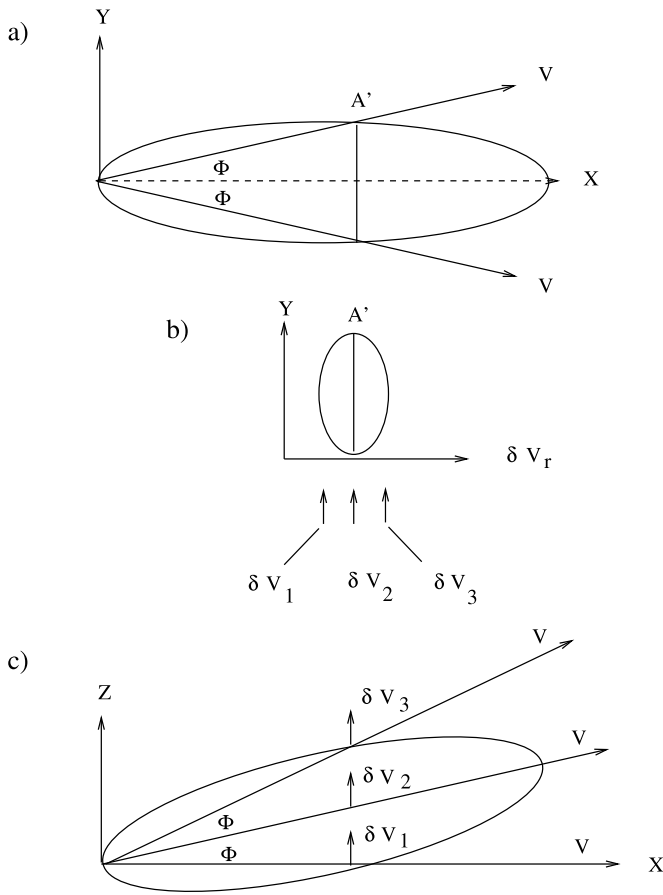


FIG. 13.—Schematic summary of the measurements from Meaburn & Walsh (1980b) along the band marked A' in Fig. 2a. (a) Image ($[X, Y]$ plane) of the northwestern lobe, which at A' (see Fig. 2a) is expanding away from the star at velocity V and an angle to the lobe axis of ϕ . (b) Measured velocity ellipse along the lobe diameter, with radial velocity differences with respect to V_{sys} . (c) Geometry of the northwestern lobe perpendicular (Z -dimension) to the plane of the sky, assuming that the northwestern lobe has a circular section and that its nearside edge is flowing at V along the X -axis in the plane of the sky.

high-speed features most likely originate within diffuse material near the nebular core. The broad velocity feature from position C extends to $V_{\text{hel}} = 120 \text{ km s}^{-1}$, where the slit crosses a diffuse “ring” seen in the 3.6 m image of Corradi referenced in § 3.2. This behavior is very similar to that observed for Mz 3 (Fig. 3 of Meaburn & Walsh 1985; Santander et al. 2004), where a “skirt” of material expanding around the nebular core but nearly *orthogonally* to the axis of the main bipolar lobes is shown to be present. A similar situation could prevail in NGC 6302. There is also a similar morphological structure in the ejected nebulosity surrounding the luminous blue variable star η Car (Smith 2002), which may suggest that this is a fundamental property of such outflows.

4. MODELING THE LOBES WITH THE SHAPE CODE

With the salient parameters of the northwestern lobe depicted in Figure 13 as a starting point, the SHAPE code (Steffen et al. 1996, 2005) has been used to reproduce as realistically as possible the kinematics and morphology of the broader structure of NGC 6302. In these simulations of the PV arrays along slits 1–4, a Hubble-type outflow is assumed in which V in Figure 13 is always proportional to the distance from the central stellar system and points along a vector away from it, and the measured (§ 3.2) value of ϕ is $12^\circ.8$. Note that this is a purely morphological and

kinematical model meant to establish the current structure and velocity “field” in the object. No hydrodynamics or radiation transport have been calculated.

The modeling with the SHAPE code is performed in two steps. First, the structure and kinematics are set up in the commercially available software 3DStudioMax version 7 (3DStudioMax is a registered trademark of Autodesk, Inc.). One might choose any other similar three-dimensional-modeling software, but 3DStudioMax is the one we consider most suitable for our purpose. The model data are then rendered as an image and a long-slit spectrum (PV array) in a renderer written for the purpose. For our model of NGC 6302 we assumed a velocity proportional to distance and directed radially outward; i.e., a Hubble-type velocity law.

The structure of the lobes of NGC 6302 has been synthesized by outlining them with splines on the direct images in Figures 1 and 2 and rotating them around the symmetry axis of each structure, thereby producing rotationally symmetric lobes. Since the symmetry axes are close to the plane of the sky, the deviations of the true outline from the projected one are expected to be very small. The alignments of the two narrow and two wide lobes have then been adjusted such that they coincide best with the direct image and the PV arrays. The inclination of the whole structure with respect to the plane of the sky has been adjusted according to the axis of the prominent northwestern lobe, for which we have used the value of $12^\circ.8$ away from the observer as determined in § 3.2.

Two additional structures have been included, the knotty area marked as K1 in Figure 2 and the knotty structures in the middle of the southern lobe. They have each been produced by one spheroidal surface that has been deformed by applying the noise modifier feature of 3DStudioMax in order to break the spherical symmetry and obtain a more random distribution throughout the volume. The southern structure is located entirely within the opening angle of the southern wide lobe. No attempt was made at this time to reproduce all the individual small-scale structure, although a number of synthetic knots by chance do coincide with observed knots and serve as a reference. This means that the “weather conditions” in NGC 6302 and in the model are different.

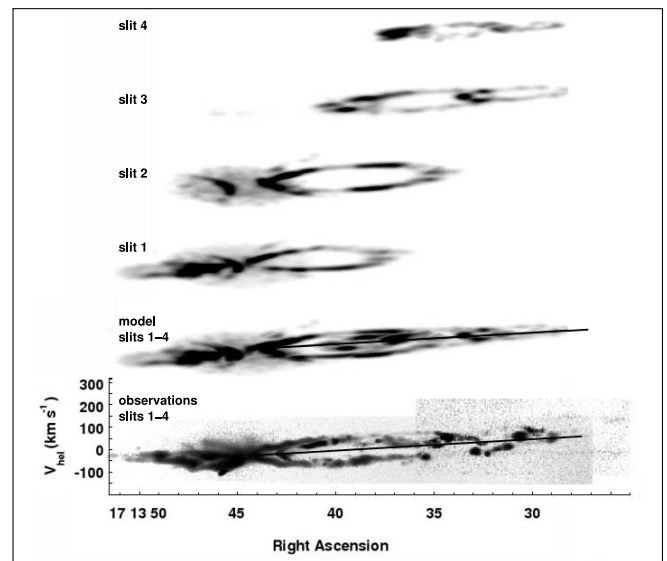


FIG. 14.—Individual PV arrays predicted by the SHAPE code for slits 1–4. Also, the superposition of the observed PV arrays for slits 1–4 is compared with the model predictions, where the tilted solid line is the expected median if Hubble-type flows prevail within the dominant northwestern lobe. The observed velocities, shown in Fig. 7, of the faint extremities (far right of the observations for slits 1–4) can be seen to deviate from this behavior significantly.

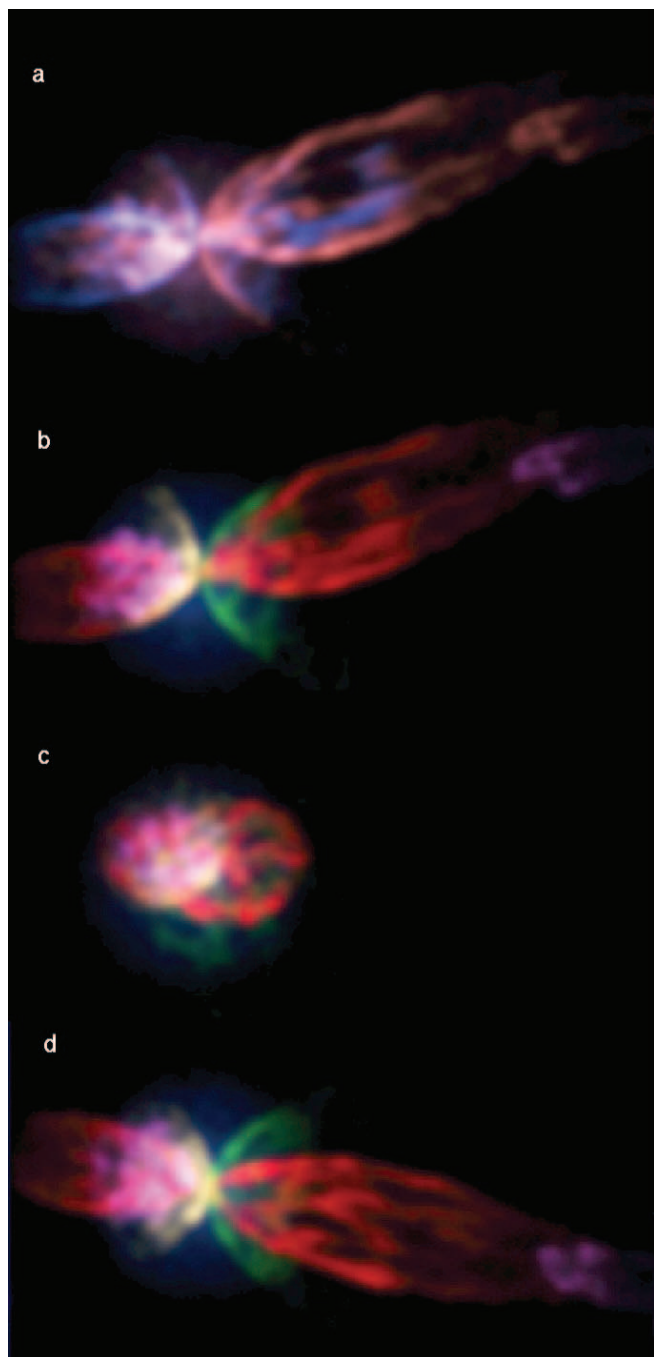


FIG. 15.—Images of NGC 6302 predicted by the SHAPE code but viewed from various directions. (*a*, *b*) Normal view along the sight line, where (*a*) is color-coded blue or red to indicate the Doppler shifts and (*b*) is color-coded arbitrarily (as are [*c*] and [*d*]) to emphasize separate structures. (*c*) North-south view in the plane of the sky. (*d*) East-west view but again in the plane of the sky (as though viewed from below the image in [*a*]).

The predicted PV arrays for slits 1–4 after this process are shown separately in Figure 14 for comparison with the observed arrays in Figures 3–7. The kinematical correspondence between the predicted and observed PV arrays is remarkably accurate. Also shown in Figure 14 is the superposition of the observed PV arrays for slits 1–4 for comparison with the modeled counterpart. The linear tilt of the axis of the outflow in these PV arrays for the prominent northwestern lobe is clear. There is only a small change in angle to the west of the knots at its extremity (of which knot 1 in Fig. 2 is one). The simulations in Figure 14 therefore

confirm conclusively that the basic outflow is Hubble-type but suggest that this flow is modified somewhat after passage through the knotty material to the extreme west of this lobe. This conformity with a Hubble-type flow pattern reinforces confidence that this present model is a true representation of NGC 6302, since such flows are found in a wide range of circumstellar phenomena.

SHAPE modeling permits for the first time different predicted views (Fig. 15) of the lobes of NGC 6302 along various axes; similar objects at less advantageous orientations (“nature” is random in this respect) can then be recognized. These illustrations should then help when determining the structures of other polypolar PNe from the multitude of complex shapes found when these are imaged.

The first two images are taken along the line of sight (Figs. 15*a* and 15*b*) and are the normal view of the object, whereas those in Figures 15*c* and 15*d* are views from within the plane of the sky along the north-south and east-west axes, respectively. The color coding for Figure 15*a* corresponds to the red-blue Doppler shifting, whereas for the rest the color coding is arbitrary to allow the separate regions of the object to be distinguished.

5. WIND-DRIVEN VERSUS BALLISTIC OUTFLOWS

There are two leading possibilities for the creation of the bipolar lobes of NGC 6302. In the first by Cantó (1978), Meaburn & Walsh (1980*b*), and Barral & Cantó (1981), an isotropic particle wind from the central star embedded in a dense disk first forms bipolar, pressure-driven cavities perpendicular to this disk. These cavities are delineated by standing shocks across which the wind refracts to drive outflows parallel to the cavity walls. Alternatively, the bipolar lobes are simply the ballistic consequences of an explosive event in the central stellar system.

The wind model has many attractions, not least that it predicts the dense knots (K1, etc.; Fig. 2*a*) found at the “acute tip” (Barral & Cantó 1981) of the northwestern lobe of NGC 6302. Within this model the outflowing cavities in the extremities of the northwestern lobe (Figs. 7–10) are predicted as the wind-driven, outflowing cavity walls first collide at this tip and then expand outward again at higher speed.

However, several objections to the wind-driven model have since arisen both here and elsewhere. Most significantly, Feibelman (2001) finds direct evidence of only a very weak wind in the nebular core with a low terminal velocity of $\sim 520 \text{ km s}^{-1}$. Meaburn & Walsh (1980*b*) show that for a distance to NGC 6302 of $\geq 150 \text{ pc}$, such a weak wind would be insufficiently energetic to form the cavities and then drive the bipolar outflows (the distance of NGC 6302 given in § 3.3 is 1.04 kpc). The observed fragmentation of the lobe walls would surely also indicate that wind formation of pressure-driven cavities has not occurred. Furthermore, the velocity vectors as depicted in Figure 13 and used throughout the convincing modeling illustrated in Figure 14 point back to the central star even where the lobe walls appear parallel (e.g., A' in Fig. 2). The velocity ellipses in the PV arrays across the lobe diameters (Meaburn & Walsh 1980*b*) are a direct consequence of this behavior and could not be produced by flows along the parallel walls of the wind-driven cavity defined by standing shocks. Elongated wind-driven cavities still in a state of pressure-driven expansion, combined with wind-driven flows parallel to their walls, need to be explored dynamically to see whether or not the present observed kinematics can be generated, i.e., velocity ellipses across the lobe diameters combined with Hubble-type outflows.

However, the Hubble-type velocity field predicted by the modeling in Figure 14, combined with these vectors pointing

back to the central star, favors the formation of the northwestern lobe by a single eruptive event. A dynamical age for this event of D (kpc) \times 1800 yr is determined for $V = 263 \text{ km s}^{-1}$ at A' in Figures 2a and 13. With the value of $D = 1.04 \text{ kpc}$ measured in § 3.3, this age becomes $\approx 1900 \text{ yr}$. This suggestion, however, leaves the creation of the complex motions at the extremities of the northwestern lobe (west of K1 in Fig. 2a) not easily explained, other than that they could perhaps be a consequence of the fastest parts of the same eruptive event (§ 4) overrunning preexisting dense knots. A simple consequence of the Hubble-type flows revealed in Figure 14 is that the outflow velocity will reach $V \approx 460 \text{ km s}^{-1}$ (Fig. 13) at the farthest extent of the northwestern lobe 3'.0 from the central star. Beyond this, at 3'.9 from the central star along the same axis, the Hubble-type law prevails but with a steeper slope, in which case $V \geq 600 \text{ km s}^{-1}$ is predicted for the faintest extremities of this northwestern outflow from NGC 6302. This is similar to the high maximum speeds ($\geq 500 \text{ km s}^{-1}$) found for the bipolar lobes of He2-111 (Meaburn & Walsh 1989) and for the ejected knots from MyCn 18 (Bryce et al. 1997).

Incidentally, the bipolar lobes of the PN Mz 3 (Meaburn & Walsh 1985) have exactly the same characteristics as those of NGC 6302, i.e., velocity ellipses are found across their lobe diameters and the lobe outflows are Hubble-type (see Fig. 4 of Meaburn & Walsh 1985; Santander et al. 2004). In the case of Mz 3, any wind could not impinge on the lobe walls, since there are dense, inner, slowly expanding shells shielding the outer extensive lobes. An ejection event within the central stellar system, shown to possibly consist of two stars by Smith (2003), with a symbiotic nature suggested by Bains et al. (2004), is similarly favored for the creation of the Mz 3 lobes.

The nature of the central source of NGC 6302 remains unknown. The extremely high electron temperature in the nebula points toward a very massive progenitor, although Casassus et al. (2000) estimate a progenitor mass between 4 and 5 M_{\odot} . Recently, Matsuura et al. (2005) detected an infrared source at the location of the central star of NGC 6302 but were unable to obtain additional information on the source's nature. Although there are no

direct indications of the central source being a binary system, the complex morphology of this nebula, with several systems of bipolar axes tilted with respect to each other, such as in NGC 2440 (López & Meaburn 1998), and its eruptive nature revealed here certainly suggests this possibility, which should be explored further in the infrared regime with adaptive optics techniques.

6. CONCLUSIONS

1. The prominent northwestern lobe of NGC 6302 has a circular section whose walls are shown to follow very precisely a Hubble-type outflow.

2. At 1'.71 from the central stellar system, the flow velocity of this northwestern lobe is measured as 263 km s^{-1} with a lobe tilt to the sky of $12^{\circ}8$.

3. A nebulous knot in the northwestern lobe, at 2'.24 from the center, has a proper motion outward of $70.4 \pm 11 \text{ mas yr}^{-1}$. The consequent expansion proper-motion distance to NGC 6302 is then $1.04 \pm 0.16 \text{ kpc}$.

4. An eruptive event 1900 years ago created the prominent northwestern lobe and possibly many of the other lobe structures.

5. High positive velocity wings to the [N II] $\lambda 6584$ line profiles to the north of the dark waist of NGC 6302 suggest the presence of an orthogonal "skirt" as found in Mz 3 (and η Car).

6. The western extremities of the northwestern lobe exhibit a small change in the slope of the Hubble-type flow, suggesting that a collision with preexisting globules of gas has occurred that modifies the outflow.

7. The outflow velocity at the extreme position of the northwestern lobe reaches $\geq 600 \text{ km s}^{-1}$.

The authors wish to thank the staff of the SPM telescope (Mexico) for their help during these observations. J. A. L. and W. S. gratefully acknowledge financial support from CONACYT (Mexico) grants 32214-E and 37214 and DGAPA-UNAM IN114199 and IN111803. M. F. G. is grateful to PPARC for his research studentship.

REFERENCES

- Aller, L. H., Ross, J. E., Omara, B. J., & Keyes, C. D. 1981, MNRAS, 197, 95
 Ashley, M. C. B., & Hyland, A. R. 1988, ApJ, 331, 532
 Bains, I., Redman, M. P., Bryce, M., & Meaburn, J. 2004, MNRAS, 354, 549
 Barnard, E. E. 1907, Astron. Nachr., 173, 123
 Barral, J. F., & Cantó, J. F. 1981, Rev. Mex. AA, 5, 101
 Barral, J. F., Cantó, J., Meaburn, J., & Walsh, J. R. 1982, MNRAS, 199, 817
 Bryce, M., López, J. A., Holloway, A. J., & Meaburn, J. 1997, ApJ, 487, L161
 Cantó, J. 1978, A&A, 70, 111
 Casassus, S., Roche, P. F., & Barlow, M. J. 2000, MNRAS, 314, 657
 Danziger, I. J., Frogel, J. A., & Persson, S. E. 1973, ApJ, 184, L29
 Elliott, K. H., & Meaburn, J. 1977, MNRAS, 181, 499
 Evans, D. S. 1959, MNRAS, 119, 150
 Feibelman, W. A. 2001, ApJ, 550, 785
 Gómez, Y., Moran, J. M., Rodríguez, L. F., & Garay, G. 1989, ApJ, 345, 862
 King, D. J., Scarrott, S. M., & Shirt, J. V. 1985, MNRAS, 213, 11
 López, J. A., & Meaburn, J. 1983, MNRAS, 204, 203
 ———. 1998, ApJ, 493, 803
 Matsuura, M., Zijlstra, A. A., Molster, F. G., Waters, L. B. F. M., Nomura, H., Sahai, R., & Hoare, M. G. 2005, MNRAS, 359, 383
 Meaburn, J., Blundell, B., Carling, R., Gregory, D. F., Keir, D., & Wynne, C. G. 1984, MNRAS, 210, 463
 Meaburn, J., López, J. A., Bryce, M., & Mellema, G. 1996, A&A, 307, 579
 Meaburn, J., López, J. A., Gutiérrez, L., Quiróz, F., Murillo, J. M., Valdéz, J., & Pedrayez, M. 2003, Rev. Mex. AA, 39, 185
 Meaburn, J., & Walsh, J. R. 1980a, MNRAS, 191, 5
 ———. 1980b, MNRAS, 193, 631
 ———. 1985, MNRAS, 215, 761
 ———. 1989, A&A, 223, 277
 Minkowski, R., & Johnson, H. M. 1967, ApJ, 148, 659
 Oliver, J. P., & Aller, L. H. 1969, ApJ, 157, 601
 Pottasch, S. R., Preite-Martinez, A., Olon, F. M., Raimond, E., Beintema, D. A., & Habing, H. J. 1985, A&A, 143, L11
 Rodríguez, L. F., et al. 1985, MNRAS, 215, 353
 Santander-García, M., Corradi, R. L. M., Balick, B., & Mampaso, A. 2004, A&A, 426, 185
 Schmeja, S., & Kimeswenger, S. 2001, A&A, 377, L18
 Smith, N. 2002, MNRAS, 337, 1252
 ———. 2003, MNRAS, 342, 383
 Steffen, W., Holloway, A. J., & Pedlar, A. 1996, MNRAS, 282, 1203
 Steffen, W., López, J. A., & Riesgo, H. 2005, Rev. Mex. AA Ser. Conf., in press